Weierstraß-Institut
für Angewandte Analysis und Stochastik

im Forschungsverbund Berlin e.V.

Preprint ISSN 0946 – 8633

Mathematical modelling of indirect measurements in periodic diffractive optics and scatterometry

Hermann Gross[1], Regine Model[1], Markus Bär[1], Matthias Wurm[2],

Bernd Bodermann[2], Andreas Rathsfeld[3]

submitted: 10th February 2006

[1] Department 8.4
Mathematical Modelling and Data Analysis
Physikalisch-Technische Bundesanstalt
Abbestraße 2-12
10587 Berlin
Germany
E-Mail: Hermann.Gross@ptb.de
Regine.Model@ptb.de
Markus.Baer@ptb.de

[2] Department 4.2
Imaging and Wave Optics
Physikalisch-Technische Bundesanstalt
Bundesallee 100
38116 Braunschweig
Germany
E-Mail: Matthias.Wurm@ptb.de
Bernd.Bodermann@ptb.de

[3] Weierstrass Institute for Applied Analysis
and Stochastics
Mohrenstraße 39
10117 Berlin
Germany
E-Mail: rathsfeld@wias-berlin.de

No. 1099

Berlin 2006

1991 *Mathematics Subject Classification.* 78A46, 65N30, 65K10.

Key words and phrases. Indirect measurements, mathematical modelling, inverse methods, diffractive optics.

Edited by
Weierstraß-Institut für Angewandte Analysis und Stochastik (WIAS)
Mohrenstraße 39
10117 Berlin
Germany

Fax: + 49 30 2044975
E-Mail: preprint@wias-berlin.de
World Wide Web: http://www.wias-berlin.de/

Abstract

In this work, we illustrate the benefits and problems of mathematical modelling and effective numerical algorithms to determine the diffraction of light by periodic grating structures. Such models are required for reconstruction of the grating structure from the light diffraction patterns. With decreasing structure dimensions on lithography masks, increasing demands on suitable metrology techniques arise. Methods like scatterometry as a non-imaging indirect optical method offer access to the geometrical parameters of periodic structures including pitch, side-wall angles, line heights, top and bottom widths. The mathematical model for scatterometry is based on the Helmholtz equation derived as a time-harmonic solution of Maxwell's equations. It determines the incident and scattered electric and magnetic fields, which fully specify the light propagation in a periodic two-dimensional grating structure. For numerical simulations of the diffraction patterns, a standard finite element method (FEM) or a generalized finite element method (GFEM) is used for solving the elliptic Helmholtz equation. In a first step, we performed systematic forward calculations for different varying structure parameters to evaluate the applicability and sensitivity of different scatterometric measurement methods. Furthermore our programs include several iterative optimization methods for reconstructing the geometric parameters of the grating structure by the minimization of a functional. First reconstruction results for different test data sets are presented.

1 Introduction

The investigation of micro- or nano-structured surfaces regarding their structure geometries and dimensions can be performed in a rapid and non-destructive way by the measurement and analysis of light diffraction from the structured surfaces. Non-imaging metrology methods like scatterometry are in contrast to optical microscopy non diffraction limited and they grant access to the geometrical parameters of periodic structures like structure width (CD), pitch, side-wall angle or line height [1, 2]. An important application of scatterometric metrology is the evaluation of structure dimensions on photo-masks and wafers in lithography [3, 4]. In particular in the semiconductor industry both the feature sizes and the required measurement uncertainty decrease continously. On the other hand conventional microscopical metrology techniques like atomic force, electron or optical microscopy unfortunately do not necessarily yield the same results. Therefore scatterometry is an important independent measurement technique for the characterization of such structures. However, scatterometric methods are not necessarily unambiguous. Typically a-priori information is required, which allows to confine the variation intervals of the structure parameters to be determined. These measurement techniques depend crucially on a high precision rigorous (i.e. vectorial and 3D) modelling of the light-structure interaction. Furthermore to determine the structure parameters from a measured diffraction pattern the inverse diffraction problem [5] is to be solved. Except for the problem of unambiguity this is strongly related to optimization problems for the development of diffractive optics (cf. [6]).

The mathematical modelling of scatterometry requires the computation of the relation between the input (the incoming wave) and output (diffraction efficiencies, phase shifts). These quantities are described by a model based on Maxwell's equations [7, 8]. For the numerical solution of the resulting Helmholtz equation there exists a whole variety of different methods. The most common ones are probably the rigorous coupled wave analysis (cf. [9, 10]) and the so-called C method (cf. [11]), whereas the integral equation method is the fastest for profile gratings (cf. the references in [12]). On the other hand, the most flexible mathematical method to solve boundary value problems for elliptic partial differential equations is the finite element method (FEM). FEM has been applied to gratings e.g. by Urbach [13], Bao [14], and Elschner et al [15]. Apart from the forward computations of the Helmholtz equation, the solution of the inverse problem, *i.e.* the reconstruction of the grating profile from measured data, is desirable. Our approach here employs a FEM-based optimization procedure [16].

This paper is organized as follows: A brief overview on non-imaging methods and the measurement systems will be given in section 2. One of the most common geometrical configurations for diffractive optical structures is a periodic pattern etched into the surface of an optical substrate, such as the trapezoidal shaped grating with two layered material components shown in section 2. The grating pattern is often created with a sequential photolithographic mask-etch process, sometimes combined with the deposition of additional material layers. In sections 3 and 4 we give a brief description of the mathematical model and the numerical algorithms which are used to determine the diffraction of light by two-dimensional grating structures. The mathematical models used are based on time-harmonic waves. Scattering of time-harmonic waves from infinite periodic structures is a classical problem, dating back to the Rayleigh expansion of the scattered field. In section 5 we employ the program package DIPOG (cf. [17]) to analyse the variability of the diffraction intensity pattern of trapezoidal shaped gratings in dependence on the different control parameters. The latter include the frequency and direction of the incident light and particularly the dimensions and optical constants of the grating geometry. DIPOG includes several iterative optimization methods for the reconstruction of the grating shape from a given set of the diffraction pattern. In contrast to shape design problems we are interested here in the shape reconstruction from given diffraction patterns. In section 6 the reconstruction results for several test data sets will be presented and discussed. In particular, we are considering aspects of the validation such as the accuracy of reconstruction in dependence on the given diffraction pattern. We will end up in a discussion of further research and open questions.

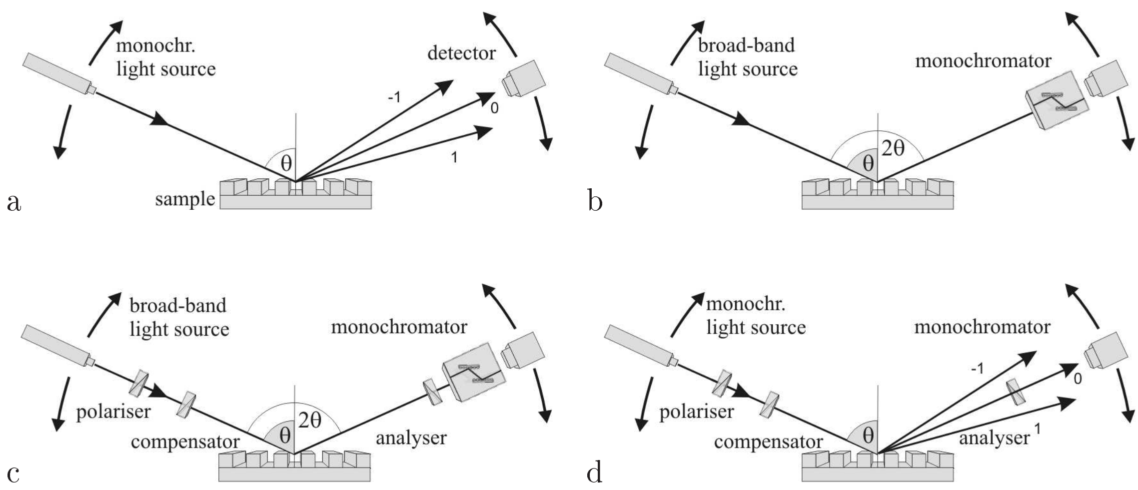

Figure 1: Schemes of different scatterometric setups:
a) standard scatterometry b) spectroscopic reflectrometry
c) spectroscopic ellipsometry d) ellipsometric scatterometry

2 Scatterometric measuring setups and test samples

Scatterometry is defined as a measurement technique for a quantitative evaluation of surface properties by angle-resolved characterisation and analysis of light scattered from a surface under test. Since no imaging optics is used, the surface and shape have to be reconstructed from intensity and/or polarisation data detected in the far field. Several measurement modes can be classified as scatterometric techniques. In Figure 1 four basic set-ups are sketched. These are standard scatterometer, spectroscopic reflectometer, spectroscopic ellipsometer, and ellipsometric scatterometer.

A standard scatterometer (Figure 1a) is used for one-dimensional periodically structured surfaces and the diffraction patterns are recorded. In the simplest case only planar diffraction is considered (classical mount). A monochromatic light source with a fixed state of polarisation is used. The polarisation is called transverse electric (TE) if the incident E-field is parallel to the grooves of the grating (also called s-polarised) and transverse magnetic (TM) if the E-field is perpendicular to the grooves (also called p-polarised). The angle of incidence θ is a parameter of the experiment that is kept constant during the measurement. Depending on the optical constants of the sample under test the measurement can be performed not only in reflexion but also in transmission mode.

In addition, reflectometry measurements can be realised with such an instrument. Here the light source and the detector are moved simultaneously in such a way that the detector position is always at an angle $-\theta_{inc}$ measured from the normal of the surface. In spectral reflectometry (Figure 1b) both the angle of incidence θ_{inc} and the angular position of the detector (at $-\theta_{inc}$) are kept constant and the measurement is done by varying the inspection wavelength (e.g. by using a tuneable laser system or a broad-band light source and a monochromator as shown here). By adding polarisation optics this set-up can be enhanced to a spectroscopic ellipsometer (Figure 1c). For this a polariser in front of the light source and another one, working as an analyser, in front of the detector is needed. Optionally a compensator/retarder (usually a quarter-wave plate, QWP) is placed in the optical path between both polarisers (either before or after the sample). With a spectroscopic ellipsometer the influence of the sample on a defined polarisation state of the incident light can be measured as a function of the inspection wavelength.

In ellipsometric scatterometry (Figure 1d) again this influence on the polarisation state of the 0^{th} diffraction order is measured but with respect to the angle of incidence and at a fixed wavelength. The ellipsometric measurands Ψ and Δ describe the state of polarisation. They are defined by the fundamental equation of ellipsometry

$$\tan\Psi e^{i\Delta} = \frac{r_p}{r_s}$$

with r_p and r_s being the complex Fresnel reflexion coefficients for p- and s-polarised light, respectively. When performing measurements in transmission mode the coefficients have to be replaced accordingly by the Fresnel transmission coefficients.

At PTB, two scatterometric set-ups are available [18]: A standard scatterometer operating at a wavelength of 633 nm, and a spectroscopic reflectometer which especially can be used for measurements in the EUV range. The sample under test we discuss here is a Chrome on Glass (CoG) mask. Their nominal geometrical parameters can be taken from Figure 2 where the grating structure is shown. In the photolithographic imaging process CoG masks are used in transmission mode. To reduce interreflexions, the Chrome absorber is anti-reflexion coated with CrO. Thus three optical efficacious materials have to be taken into account: Cr, CrO, and the fused silica substrate (SiO_2). Their complex indices of refraction for wavelengths of 13.58 nm, 193 nm, and 632.8 nm are given in table 1.

3 Mathematical modelling of scatterometry

In the previous section a special structure, the CoG1 mask is described. Ideally, an optical grating is an infinite plate consisting of different non-magnetic materials with permeability μ_o and dielectric constants ϵ. The functional relation between the input (the incoming wave) and output (diffraction efficiencies, phase shifts) can be described by a mathematical model based on Maxwell‘s equations [7, 8]. It depends on the one hand on the parameters of the incoming wave, the wavelength λ and the angle of incidence $\theta \in (-\pi/2, \pi/2)$, and on the other hand on the mask parameters, i.e. the refraction indices and the geometric parameters of the grating. The coordinate system is chosen as follows (cf. Figure 2): the material distribution is supposed to be periodic with period d in x direction and homogeneous parallel to the grooves in z direction. Hence, ϵ is invariant with respect to z, and the y-axis is perpendicular to the plate.

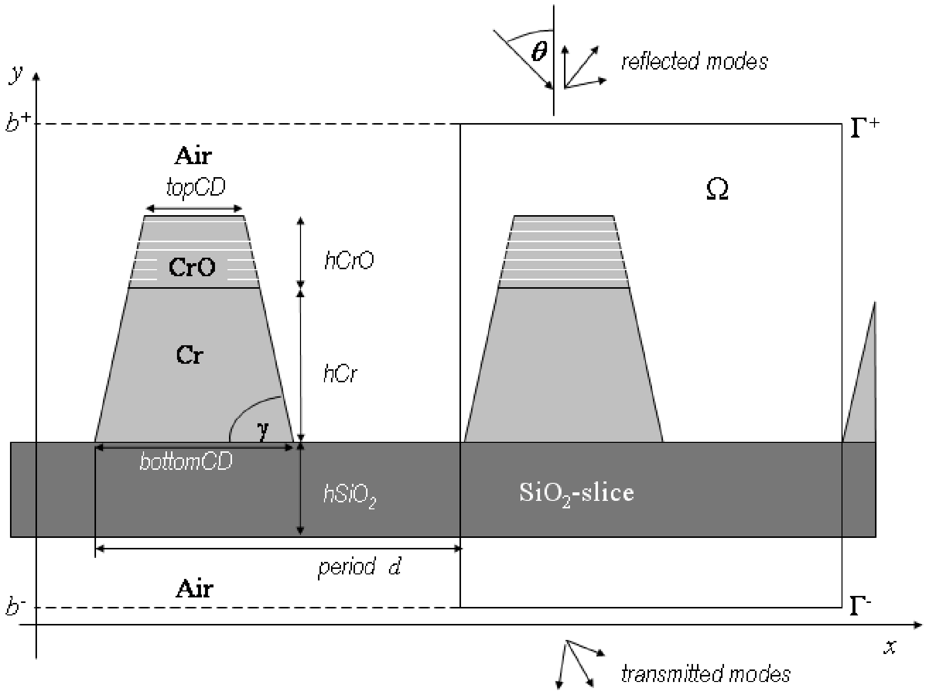

Figure 2: CoG1 grating – Chrome on Glass mask used for forward calculations and reconstructions ($d = 1120$ nm, $\gamma = 73°$, $hSiO_2 = 6.35$ mm, $hCr = 50$ nm, $hCrO = 23$ nm)

For simplicity, the upper cover material is assumed to be air and the incident wave is normalised to have unit amplitude. Unlike the generalized (conical) case, classical diffraction deals with incident wave directions restricted to the x-y plane resulting in reflected and transmitted plane wave modes in the x-y plane, too. Then in case of polarized incident light the wave is a superposition of TE and TM polarized light. Note that in the TM resp. TE case the magnetic field **H** and the electric field **E** remain parallel to the grooves so that the transverse component of **H** in the TM case and the transverse component of **E** in the TE case can be determined from the two-dimensional Helmholtz equation

$$\Delta u + k^2 u = 0 \tag{1}$$

with the piecewise constant wave number function $k = k(x, y) = \omega\sqrt{\mu_0 \epsilon(x, y)}$ and angular frequency ω of the incident light wave. On material interfaces the solution u and its normal derivative $\partial_n u$ for TE polarisation resp. the solution u and the product $k^{-1}\partial_n u$ for TM polarisation have to cross the interface continuously. In the infinite regions the usual outgoing wave conditions for half spaces are required. Therefore, the domain Ω in the cross section plane for the FEM solution of Eq. (1) can be reduced to a rectangle with the x coordinate varying between zero and the period d and with two artificial boundaries $\Gamma^{\pm} = \{y = b^{\pm}\}$ (cf. Figure 2). For

(1), a boundary value problem on Ω is to be solved with quasi-periodic boundary condition $u(0, y) = u(d, y)\exp(-i\alpha_0 d)$, on the lateral boundary part and with non-local boundary conditions on $\Gamma^{\pm}$. For instance on Γ^+, this non-local boundary condition means that the trace $\partial_n u|_{\Gamma^+}$ on Γ^+ of the normal derivative $\partial_n u$ must equal the y derivative of the Rayleigh expansion (cf. Eq. (2)) of the trace $u|_{\Gamma^+}$ of u from Ω. The Rayleigh expansion is a special case of the Fourier series expansion of $u = E_z$ at the horizontal boundaries. E.g. in the case of TE polarisation it is of the form

$$E_z(x, b^+) = \sum_{n=-\infty}^{\infty} A_n^+ \exp(+i\beta_n^+ y)\exp(+i\alpha_n x) + A_0^{inc}\exp(-i\beta_o^+ y)\exp(+i\alpha x)\ , \quad (2)$$

$$E_z(x, b^-) = \sum_{n=-\infty}^{\infty} A_n^- \exp(+i\beta_n^+ y)\exp(+i\alpha_n x) \quad (3)$$

with $k^{\pm} = k(x, b^{\pm})$, $\alpha_n = k^+ \sin\theta + \frac{2\pi}{d}n$ and $\beta_n^{\pm} = \sqrt{(k^{\pm})^2 - (k^+ \sin\theta + \frac{2\pi}{d}n)^2}$, and $A_0^{inc} = 1$. The important Rayleigh coefficients $A_n^{\pm}$are those with $n \in U^{\pm}$,

$$U^{\pm} = \begin{cases} \left\{n \in Z : |\alpha_n| < k^{\pm}\right\} & \text{if Im } k^{\pm} = 0 \\ \emptyset & \text{if Im } k^{\pm} > 0\ . \end{cases}$$

Indeed, they describe magnitude and phase shift of the propagating plane waves. More precisely, the modulus $|A_n^{\pm}|$ is the amplitude of the nth reflected resp. transmitted wave mode and $\arg(A_n^{\pm}/\,|A_n^{\pm}|)$ the phase shift. The terms with $n \notin U^{\pm}$ lead to evanescent waves only. The optical efficiencies of the grating can be measured and are determined by

$$e_n^{\pm} = \frac{\beta_n^{\pm}\,|A_n^{\pm}|^2}{\beta_o^+\,|A_0^{inc}|^2}\ . \quad (4)$$

with $(n, \pm) \in \{(n, +) : n \in U^+\} \cup \{(n, -) : n \in U^-\}$. The coefficients of the Rayleigh expansion are computed from the FEM solution of Eq. (1). Then, the optical efficiencies are obtained from Eq. (4). Note that the efficiency of a transmitted or reflected mode is nothing else but the portion of energy transferred from the incoming light to this mode. The efficiencies in case of TM polarisation are derived analogously.

4 Numerical algorithms for solving the Helmholtz equations and the reconstruction problem

For the numerical solution of the boundary value problem from the last section, there exists a whole variety of different methods. The most popular are probably the rigorous coupled wave analysis (cf. [9]) and the so-called C method (cf. [11]), whereas the integral equation method is probably the fastest for profile gratings (cf. the references in [12]). On the other hand, the most general mathematical method to solve boundary value problems for elliptic partial differential equations is the finite element method (FEM). The advantage of FEM is that it is capable to simulate the diffraction by gratings with general geometry due to existing general triangulation programs. No approximation of the domain Ω by a union of rectangular subdomains is needed, and no critical Rayleigh expansion is used. FEM has been applied to gratings e.g. by Urbach [13], Bao [14], and Elschner et al [15].

To set up the numerical scheme of finite elements, the first step is to derive a variational reformulation of the boundary value problem for the Helmholtz equation (1). Formally, a test function v is introduced over Ω. Multiplying (1) by the complex conjugation of v and integrating over Ω yields $\int_\Omega\{\Delta u+k^2u\}\overline{v}=0$ for all v. Applying the Gauß integration formula and taking into account the boundary and transmission conditions, the variational formulation equivalent to the boundary value problem of (1) over Ω is obtained. For instance, in the case of the classical TM polarization this yields

$$\int_\Omega \frac{1}{k^2}\nabla u\cdot\overline{\nabla v}-\int_\Omega u\overline{v} \;+\; \frac{1}{(k^+)^2}\int_{\Gamma^+}(T_\alpha^+ u)\overline{v}+\frac{1}{(k^-)^2}\int_{\Gamma^-}(T_\alpha^- u)\overline{v} \;= \\ -\;\frac{1}{(k^+)^2}\int_{\Gamma^+}(2\mathrm{i}\beta e^{\mathrm{i}\{\alpha x-\beta y\}})\overline{v},\quad v\in H_p^1(\Omega)\,. \tag{5}$$

Here $H_p^1(\Omega)$ stands for the first order Sobolev space of quasiperiodic functions and $T_\alpha^\pm$ is the non-local operator mapping a trace function u on $\Gamma^\pm$ to the y-derivative of its Rayleigh expansion (2) resp. (3).

Having derived a variational equation like (5), the FEM is obtained by approximating u with u_h from a finite element space $S_h\subseteq H_p^1(\Omega)$ and by restricting also the test functions $v=v_h$ to S_h. More precisely, the FEM seeks the approximate solution u_h solving

$$\int_\Omega \frac{1}{k^2}\nabla u_h\cdot\overline{\nabla v_h}-\int_\Omega u_h\overline{v_h} \;+\; \frac{1}{(k^+)^2}\int_{\Gamma^+}(T_\alpha^+ u_h)\overline{v_h}+\frac{1}{(k^-)^2}\int_{\Gamma^-}(T_\alpha^- u_h)\overline{v_h} \;= \\ -\;\frac{1}{(k^+)^2}\int_{\Gamma^+}(2\mathrm{i}\beta e^{\mathrm{i}\{\alpha x-\beta y\}})\overline{v_h},\ v_h\in S_h\,. \tag{6}$$

The space S_h is the collection of all continuous and piecewise linear functions subordinate to a given triangulation of Ω. By h we denote the mesh size of the triangulation, i.e. the maximal diameter of the subtriangles of Ω. Clearly, the smaller h is, the better the function u can be approximated by u_h. However, smaller h results in a larger number of subtriangles and in a higher dimension of the vector space S_h which increases the computational effort to solve (6). If u_h is determined, then instead of u the approximation u_h is expanded into the Rayleigh series on the right-hand sides of (2) and (3). This way approximate values of the Rayleigh coefficients are generated and, using (4), the efficiencies can be computed.

The FEM works well if the ratio period over wave length is moderate. However, if the last ratio is large, the solution u is oscillatory and a tiny mesh size h together with an unacceptably long computing time is needed to produce a reasonable approximation. Better results are possible with the generalized FEM (GFEM). Here the only difference between FEM and GFEM is a different trial space S_h of approximate functions. In the case of GFEM the trial space consists of continuous functions the restrictions of which to the subtriangles of the triangulations are special solutions of the Helmholtz equation. More precisely, they are piecewise approximate solutions since there are no explicit Helmholtz solutions with prescribed boundary data even for simple domains as triangles.

For the optimal design of gratings (compare e.g. [16, 8]), the starting point is a functional f defined on the set of gratings and expressing the objective of the optimization task. This can be any user defined linear or quadratic expression of the grating efficiencies and phase shifts. For example,

$$f(\text{grating}) := \sum_{(n,\pm):n\in U^\pm} \Big\{ a_n^\pm e_n^\pm + b_n^\pm [e_n^\pm - c_n^\pm]^2 \Big\}, \tag{7}$$

where the constants $a_n^\pm$, $b_n^\pm$, and $c_n^\pm$ are fixed by the user. Of course, the terms like those in (7) may depend on several prescribed wave lengths or on several prescribed angles of incidence. The optimization of the objective functional in the class of all gratings is, from the mathematical point of view, a so-called severely ill-posed problem and even the best numerical algorithms cannot be very accurate. Therefore, the class of admissible gratings should be restricted to a subclass of gratings described by a small number of real parameters $r_j,\ j = 1, \ldots, J$. Box conditions are supposed, i.e. the admissible parameters are restricted to user prescribed intervals.

The program package DIPOG [17] can treat three classes. The first class is that of polygonal profile gratings, i.e. of gratings consisting of only two different materials separated by an interface which is described by a polygonal curve in the cross-section. In this class the x and y coordinates of the corners of the polygonal profile curve are optimized. The second class is that of stacks of a finite number of trapezoids placed one on each other (cf. Figure 2) and the parameters of optimization are the refractive indices of the trapezoid materials and the geometry parameters of the trapezoids. The last class is that of a general fixed grating geometry with a varying polygonal interface curve. Here the parameters of optimization are the refractive indices of the grating materials (except those of the substrate and cover material) and the coordinates of the corners of the polygonal interface curve.

To solve the optimization, DIPOG offers three gradient based algorithms, namely a method of augmented Lagrangian, a conjugate gradient method, and an interior point method. The algorithmic parameters of these methods must be adapted to the optimization problem by the user. Unfortunately, the gradient based algorithms are local methods, i.e. the solution of these optimization methods render local solutions only. Recall that a local minimum of an optimization problem is a set of parameters $\tilde{r}_j,\ j = 1, \ldots, J$ such that there is a small threshold ε with

$$f\Big(\{\tilde{r}_j,\ j = 1, \ldots, J\}\Big) \le f\Big(\{r_j,\ j = 1, \ldots, J\}\Big),$$

for all $\{r_j,\ j = 1, \ldots, J\}$ with $|r_j - \tilde{r}_j| < \varepsilon,\ j = 1, \ldots, J$. The optimization problems for gratings usually have a lot of local minima different from global minima. In such a case the determination of the global optimum is difficult. A restart of the optimization algorithm from various initial solutions and choosing the minimum of the local solutions can be a helpful strategy. Alternatively, DIPOG includes a global optimization algorithm of simulated annealing. This stochastic algorithm, however, can be extremely time consuming and the determination of a global solution is not guaranteed either.

An important application for the optimization tools is the reconstruction problem (cf. [8, 19]). Here a grating of a certain class is given and the corresponding material resp. geometry parameters should be reconstructed from the measured efficiencies and phase shifts of the grating. This is done by solving an optimization problem, e.g., with the objective functional

$$f\Big(\{r_j,\ j = 1, \ldots, J\}\Big) := \sum_{l=1}^{L} \sum_{m=1}^{M} \sum_{(n,\pm):n\in U^\pm} b_n^\pm(\lambda_l, \theta_m)\Big[e_n^\pm(\lambda_l, \theta_m) - c_n^\pm(\lambda_l, \theta_m)\Big]^2, \quad (8)$$

where $\lambda_l,\ l = 1, \ldots, L$ and $\theta_m,\ m = 1, \ldots, M$ are the wave lengths resp. angles of incidence of the measurement, the $c_n^\pm(\lambda_l, \theta_m)$ are the measured efficiencies, and the $b_n^\pm(\lambda_l, \theta_m) > 0$ some weight factors. Clearly, the parameter set of the sought grating is a global minimum of the non-negative objective functional. Though there is no theoretical result claiming the uniqueness of the minimal solution, one should be optimistic that the solution is unique at least for sufficiently many measured efficiencies and phase shifts. Then there is a good chance that the optimization tools of DIPOG will reconstruct the parameters of the sought grating. Of course, the accuracy depends on the measurement uncertainty and on the behavior of the mapping assigning the efficiency data to each parameter set.

5 Variation of model parameters – analysing the dynamics of the diffraction pattern

To analyse the variability of the diffraction pattern of trapezoidal shaped gratings such as CoG1, described in section 2, we employ DIPOG by calling its FEM or GFEM executables. The most important parameters are the optical indices of all material components and the geometrical dimensions of the grating structure as well as the wavelength of the incident light and its angle relative to the normal of the grating surface. The period or pitch of the grating structure is part of the geometrical dimensions.

λ	13.58 nm	193 nm	632.8 nm
CrO	0.916358+i 0.044834	1.7452+i 1.3353	3.1185+i 0.3802
Cr	0.931609+i 0.039533	1.0549+i 1.4269	3.7329+i 3.8113
SiO_2	0.977821+i 0.010901	1.5608+i 0.000000035	1.4571+i 0.00000000058

Table 1: Optical constants of the material components of CoG1 (cf. [20]) used for the calculations and shape reconstructions

The scattering of the incoming light depends strongly on the chosen parameters. In Eq. (4) the ratio of the energy of a propagating mode of the scattered waves to the energy of the incoming wave is called the efficiency of the mode. With respect to the shape reconstruction by measured efficiencies, one of the key features of any grating is the distribution of its efficiencies over the propagating modes in dependence from the model parameters. To support the 'metrological' expectations about the measurable efficiencies of photo-masks such as CoG1 (Chrome on Glass) we have performed systematic forward calculations for different control parameters. In the following we present some examples.

The Figures 3a and 3b show the simulation results for the reflected efficiency distribution of the polarization type TE if the angle of the incoming wave is changed. Here we have used the GFEM algorithms of DIPOG in order to get a sufficient accuracy also for the example with small wavelength. In Figure 3a the wavelength is fixed to 13.58 nm and in Figure 3b to 632.8 nm. The same trapezoidal grating (CoG1, see section 2) is used for all calculations: The Chrome-on-Glass mask is assumed with a bottom length of 624.6 nm, an trapezoidal angle of 73°, a height of the Cr layer of 50.0 nm and a height of the CrO layer of 18 nm. The period of the grating is 1120 nm and the SiO2 substrate has a thickness of 6.35 mm. The used optical indices for the different wavelengths are given in Table 1. In order to support a better recognition of the dynamical changes in the distribution we have chosen a 3D-presentation of the calculated results formed by a pseudo-surface of efficiencies as a function of the order of diffraction and the control parameter, which is the incidence angle in the Figures 3a and 3b. In Figure 3b one can observe increasing efficiencies with an increasing angle of the incident light. However, for the small wavelength (Figure 3a), which is comparable to the critical dimensions of the grating structure, the angular dependence of the efficiency distribution becomes more complex: The increasing efficiencies of all diffraction orders look like a modulated periodic function. The periodicity is w.r.t. θ and the period is about 8°.

Because the heights of the material layers and their top and bottom widths are crucial control parameters, the sensitivity of the efficiency pattern w.r.t. these parameters is important. Figure 4a presents the calculated efficiency pattern for a variation of the thickness of the chrome layer: Here we have chosen an intermediate wavelength of 193 nm and an incidence angle of 10°. The height hCr in Figure 2 is varied in the range from 30 to 150 nm by steps of 5 nm. A distinctive diffraction pattern with deviations in the reflected efficiencies of about one even over the step size of 5 nm can be observed.

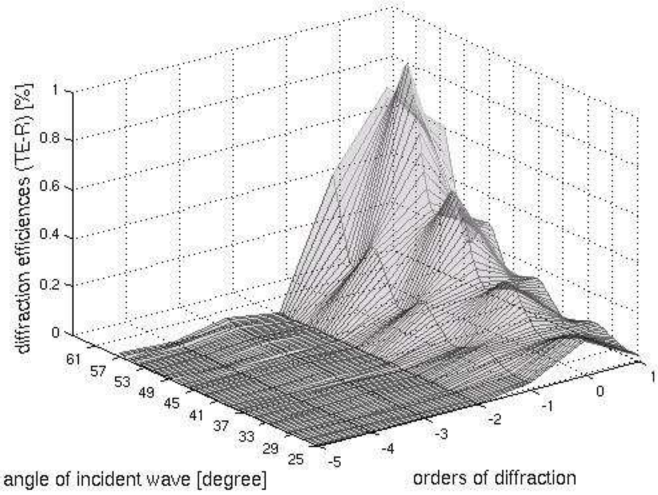

a

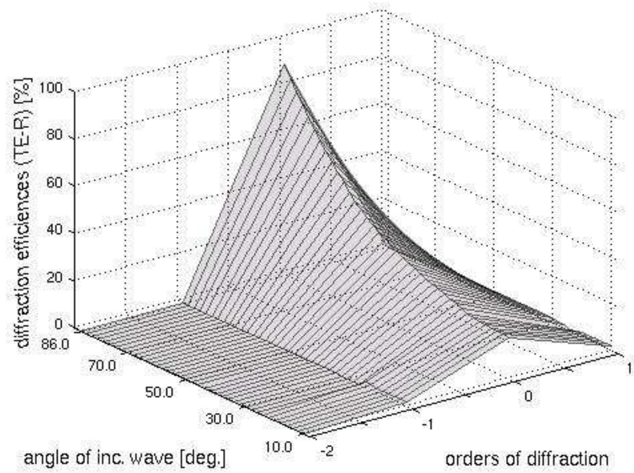

b

Figure 3: Efficiency patterns calculated for CoG1 for a variation of incidence angle θ with a) λ =13.58 nm and b) λ =632.8 nm

The sensitivity of the diffraction efficiencies w.r.t. different top and bottom widths of CoG1 is also strong as can be seen in Figure 4b. At the same sidewall angle of 73° we have changed the bottom length of the trapezoid grating CoG1 from 200 nm to 900 nm in steps of 25 nm (incidence angle and wavelength: 10° resp. 632.8 nm).

In contrast to the strong sensitivity of the efficiencies in the previous examples a variation of the real part of the refractive index of Cr leads to almost constant values.

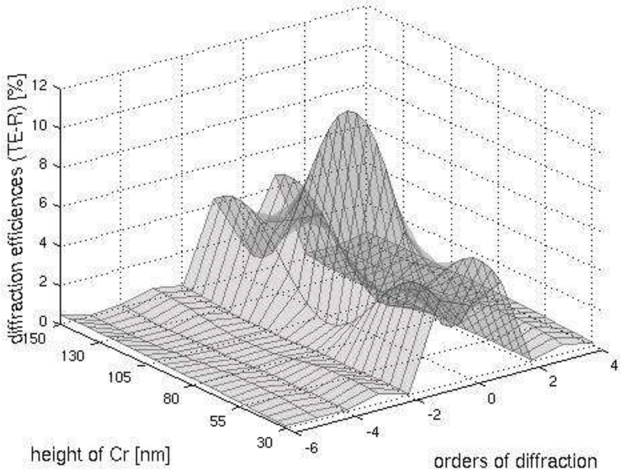

a

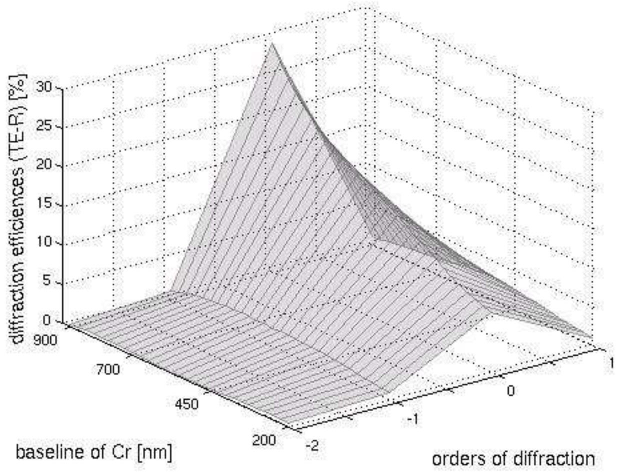

b

Figure 4: Efficiency patterns calculated for CoG1 for a) variation of hCr in CoG1 at λ=193 nm and b) variation of bottom length in CoG1 at λ=632.8 nm

6 Optimization results – reconstruction of the model parameters from simulated data sets

The shape reconstruction from a given efficiency is an inverse problem and equivalent to the minimization of an objective functional f describing the difference between a calculated and a given efficiency pattern. The examples in the previous section give some insight into the sensitivity w.r.t. the different model parameters which specify the grating structure and the inspecting light. The additive terms of the functional f in Eq. (8) depend on the efficiencies representing the known data. The number M of these terms has always to be greater or equal to the number N of the model parameters which are sought. Only if this condition is fulfilled a meaningful reconstruction can be expected.

In order to make the reconstruction feasible, we have reduced the inverse problem to the reconstruction of a finite set of geometrical parameters specifying the CoG1 mask. We fix the inspecting wavelength to 632.8 nm and calculate several efficiency patterns for different incidence angles of the inspecting light. The efficiencies were calculated with the GFEM algorithm of DIPOG at a high error level and over a triangulation different from those used in the reconstruction algorithm. Moreover we fix the optical parameters of the trapezoidal grating and those of the superstrate and substrate materials (air resp. SiO2) to the values given in Table 1. Then the following seven model parameters remain for the optimization: the bottom length of the Cr layer, the height of the Cr layer, the x coordinates of the upper left and the upper right corners of this layer, the height of the CrO layer and the x coordinates of the upper left and the upper right corners of the CrO layer. The admissible domain of these parameters has to be restricted by adding lower and upper bounds and furthermore initial values have to be provided. All the settings are declared in an ASCII-formatted input file for the optimization algorithms of the DIPOG software. At least M different values from the simulated measurement data, i.e. from the known efficiency pattern for possible different angles of incidence, have to be inserted into this input file, too. They are needed to specify the functional f. Remember, the number of measurement data should exceed the number of unknown parameters, i.e. M should satisfy the constraint $\mathrm{M} \geq 7$.

By $\mathcal{M}$ we denote the set of all possible efficiencies for all possible wavelengths, incidence angles, and diffraction orders. Clearly, for a reconstruction we use a subset of $\mathcal{M}$ with M entities of the efficiency values of the simulated measurement data. We have tested different subsets which satisfy the constraint $\mathrm{M} \geq 7$. If we choose the reflected and transmitted modes of diffraction orders 0 and -1 for the polarization types TE and TM at the four incidence angles of 10°, 15°, 30°, and 35° (M=32), a good reconstruction result is found (cf. Figure 5a). The smaller subset of the same reflected and transmitted modes (order 0 and -1, polarization TE and TM) at a single incidence angle θ of 80° (M=8) leads to a surprisingly good result for the shape reconstruction. Nevertheless, many other examined subsets did not produce acceptable results for the shape of the sought CoG1 grating and an example for such a case is shown in Figure 5b (reflected and transmitted modes of diffraction orders 0 and -1 and polarization type TE and TM at incidence angle $\theta = 75°$).

If we create new sets of known data by changing the height of the CrO layer from 23 nm to 18 nm, we find a very similar behavior. Good reconstruction results are achieved by the same subsets and particularly the new height of the CrO layer is found properly. In many cases of reconstruction all the seven parameters specifying the CoG1 mask are found with an accuracy less than 1 %.

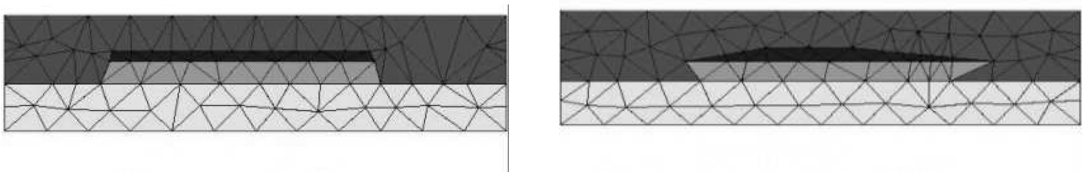

a b

Figure 5: Optimization results for simulated CoG1 test sets: a) right reconstruction by a suitable subset (M=32); optimized values for hCr: 50.04 nm (right value: 50.00 nm) and for hCrO: 23.08 nm (right value: 23.00 nm) and b) wrong reconstruction by an unsuitable subset with M=8. For details see text.

If we compare the shape of the functional f for the two subsets of the known data which are suitable for a good reconstruction, we observe the different shapes shown in Figure 6. Particularly Figure 6a exhibits a steeper descent toward the minimum in the direction of the hCr axis. In Figure 6 the functional f is calculated varying the heights hCr and hCrO of the two trapezoidal layers. The remaining five parameters are fixed to their values used for the simulation of the input data. For the selected admissible range of the two heights the coordinates of the minimum values of the objective functional are very near to the expected values of 50 nm for hCr and 18 nm for hCrO. However, they were only found if the initial value for hCrO is set to a value smaller than 60 nm where the functional f has a ridge parallel to the hCr axis. Otherwise the (second) local minimum of f on the other side of this maximum is found. Because we use gradient based optimization methods the admissible range of model parameters and their initial values can have a strong influence on the accuracy of the reconstruction result.

Besides there are further strong determinants for the 1% accuracy of the presented reconstruction results, namely the scaling factors of the model parameters. The performance of the local optimization depends on a proper scaling of the parameters which controls the size of the partial derivatives $\partial f/\partial r_i$ of the functional f in Eq. (8), where r_i with i=1,...,7 are sought-after model parameters. For instance, suppose the partial derivate $\partial f/\partial r_1$ is much larger than the other partial derivatives. Then it may happen that the small ones are not used for a correction of the iterative solution towards the local minimum. To prevent such a situation the model parameters and their lower and upper bound values have to be replaced by scaled parameters ($r_i' = s_i r_i$). Choosing the right scaling factors, the partial derivatives can be made to be almost of the same size, and the iteration converges well. The above mentioned cases of good reconstruction results can only be found with properly selected scaling factors.

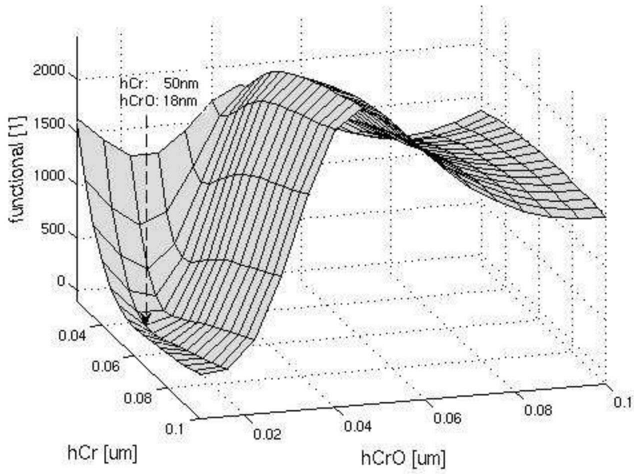

a

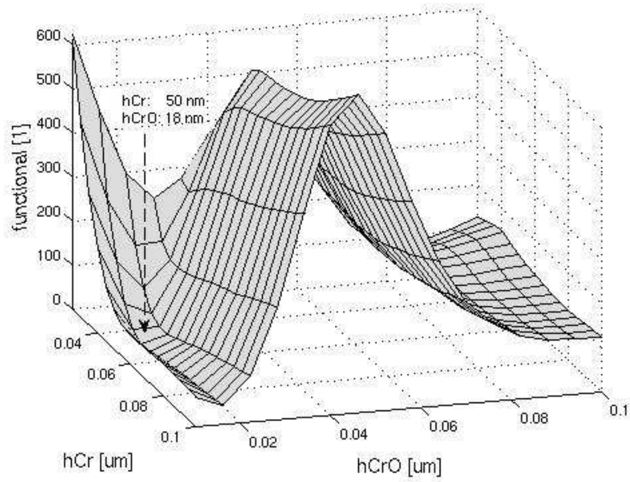

b

Figure 6: Objective functions for test case CoG1: hCr versus hCrO for the two suitable subsets with a) M=32 (4 $\theta's$: 10°,15°,30°,35°) and b) M=8 (1 θ : 80°; see text for details).

7 Discussion

We have demonstrated that the proposed generalized finite element method (GFEM), implemented in the DIPOG software enables the numerical computation of diffraction efficiencies, even if the ratio of inspecting wavelength ($\lambda = 13.58$nm) and grating period ($d = 1.12\mu m$) is in the range of $1/100$. The variability of the efficiency patterns depends on the parameters of the inspecting light and on the geometry of the scattering probe. Here we have determined these quantities for examples of trapezoidal shaped gratings typically found on CoG photolithography masks. Forward computations with systematic parameter changes have been performed in order to achieve an estimate of the sensitivity of the scattering efficiencies on the parameters specifying a "virtual experimental set-up".

In a second step, the diffraction modes computed from forward calculations have been used as input of an optimization routine aimed at reconstructing the profile of the grating. This amounts to a solution of the inverse problem that might fail if it is based upon insufficient input data. Recall that the last is always a subset chosen from the set of all available efficiencies. All together, we have tested different subsets of the modelled diffraction patterns with quite different reconstruction results. Good results, i.e. an accuracy less than 1 % for the input parameters of modelled CoG mask, were only produced for special subsets such as the scattering efficiencies of the TE and TM modes at four different angles of incidence. Subsets with a single angle of incidence in most cases are not sufficient to solve the inverse problem. Here a systematic method to find suitable subsets is still missing. Clearly, the optimal subsets of this method would also reduce the expense for the sampling of the required scatterometric measurement data. Also using additional measurands as input data like e.g. the relative phase information between the diffracted TE and TM modes (cf. ellipsometric scatterometry) could be helpful to decrease the reconstruction uncertainty.

In general, simulations are well suited to test the accuracy of optimization algorithms and inverse problem solvers designed for processing measurement data. Clearly, the determination of the uncertainty in indirect measurements relying upon inverse methods or related parametric fitting routines are a challenge in metrology, which will require a lot of further mathematical analysis and computational work. Simulations like the ones described above will be crucial to resolve these questions. In an important next step, we plan to reconstruct profiles of the gratings from experimentally measured data along the lines described above. This will provide a crucial test for the accuracy of the model and the used algorithm and may require further considerations regarding measurement noise.

References

[1] B.K. Minhas, S.A. Coulombe, S. Sohail, H. Naqvi, and J.R. McNeil, *Ellipsometric scatterometry for metrology of sub-0.1μm-linewidth structures*, Appl. Optics, **37**, No. 22 (1998), pp. 5112–5115.

[2] H.T. Huang and F.L. Terry Jr., *Erratum to "Spectroscopic ellipsometry and reflectometry from gratings (Scatterometry) for critical dimension measurement and in situ, real-time process monitoring" [Thin Solid Films 455-456 (2004) 828-836]*, Thin Solid Films, **468** (2004), pp. 1155–1169.

[3] C.J. Raymond, M.R. Murnane, S. Sohail, H. Naqvi, and J.R. McNeil, *Metrology of subwavelength photoresist gratings using optical scatterometry*, J. Vac. Sci. Technol., **13** (4) (1995), pp. 1484.

[4] C.J. Raymond, M.R. Murnane, S.L. Prins, S. Sohail, H. Naqvi, and J.R. McNeil, *Multiparameter grating metrology using optical scatterometry*, J. Vac. Sci. Technol., **15** (2) (1997), pp. 361–368.

[5] I. Kallioniemi, J. Saarinen, and E. Oja, *Optical scatterometry of subwavelength diffraction gratings: neural-network approach*, Appl. Optics, **37**, No. 25 (1998), pp. 5830.

[6] J. Turunen and F. Wyrowski (eds.), *Diffractive optics for industrial and commercial applications*, Akademie-Verlag, Berlin, 1997.

[7] R. Petit, (ed.), *Electromagnetic theory of gratings*, Springer-Verlag, Berlin, 1980.

[8] G. Bao and D.C. Dobson, *Modeling and optimal design of diffractive optical structures*, Surveys on Mathematics for Industry, **8** (1998), pp. 37–62.

[9] M.G. Moharam and T.K. Gaylord, *Rigorous coupled wave analysis of planar grating diffraction*, J. Opt. Soc. Amer., **71** (1981), pp. 811–818.

[10] A. Tavrov, M. Totzeck, N. Kerwien, and H.J. Tiziani, *Rigorous coupled-wave analysis calculus of submicrometer interference pattern and resolving edge position versus signal-to-noise ratio*, Opt. Eng., **41**(8) (2002), pp. 1886–1892.

[11] J. Chandezon, D. Maystre, and G. Raoult, *A new theoretical method for diffraction gratings and its applications*, J. Opt. (Paris), **11** (1980), pp. 235–241.

[12] B.H. Kleemann, *Elektromagnetische Analyse von Oberflächengittern von IR bis XUV mittels einer parametrisierten Randintegralmethode: Theorie, Vergleich und Anwendungen*, Dissertation, TU Ilmenau, 2002, Mensch und Buch Verlag Berlin, 2003.

[13] H.P. Urbach, *Convergence of the Galerkin method for two-dimensional electromagnetic problems*, SIAM J. Numer. Anal., **28** (1991), pp. 697–710.

[14] G. Bao, *Finite element approximation of time harmonic waves in periodic structures*, SIAM J. Numer. Anal., **32** (1995), pp. 1155–1169.

[15] J. Elschner, R. Hinder, and G. Schmidt, *Finite element solution of conical diffraction problems*, Advances in Comp. Math., **16** (2002), pp. 139–156.

[16] J. Elschner and G. Schmidt, *Numerical solution of optimal design problems for binary gratings*, J. Comput. Physics, **146** (1998), pp. 603–626.

[17] J. Elschner, R. Hinder, A. Rathsfeld, and G. Schmidt, *DIPOG Homepage*, http://www.wias-berlin.de/software/DIPOG

[18] M. Wurm, B. Bodermann, and W. Mirande, *Investigation and evaluation of scatterometric CD metrology methods*, Proc. of SPIE, **5858** (2005), 585813.

[19] J. Chandezon, A.Ye. Poyedinchuk, and N.P. Yashina, *Reconstruction of periodic boundary between dielectric media*, Mathematical Methods in Electromagnetic Theory, Conference Proceedings of MMET*02, Kiev (2002), pp. 416–419.

[20] E.M. Gullikson, *X-ray Interactions With Matter*, http://www-cxro.lbl.gov/optical_constants